Experimental Active Noise Control Using Faust On FPGA: Comparison Between A Multi-Point and Spherical Harmonics Method

Loïc Alexandre, Pierre Lecomte, Marie-Annick Galland

forum acusticum 2023

EXPERIMENTAL ACTIVE NOISE CONTROL USING FAUST ON FPGA: COMPARISON BETWEEN A MULTI-POINT AND SPHERICAL HARMONICS METHOD

Loïc Alexandre[1*] **Pierre Lecomte**[2] **Marie-Annick Galland**[1]
[1] Univ Lyon, Ecole Centrale de Lyon, CNRS, Univ Claude Bernard Lyon 1, INSA Lyon, LMFA, UMR5509, 69130, Ecully, France
[2] Univ Lyon, Univ Claude Bernard Lyon 1, CNRS, Ecole Centrale de Lyon, INSA Lyon, LMFA, UMR5509, 69622 Villeurbanne France

ABSTRACT

Active noise control over an extended area is usually performed using multi-point pressure minimization. Recent advances in approaches using spherical harmonics, i.e. ambisonics, show to be attractive to control three dimensional acoustic fields. However, to this day, only few experimental results are reported in the literature. This paper proposes a preliminary experimental multichannel active noise control system implemented on a FPGA using the Faust programming language. Two multichannel Filtered-x LMS algorithms are tested to minimize either multi-point pressure or ambisonic components of the sound field. Both methods use the same four-microphone and four-loudspeaker geometrical arrangement which allows to work with first order ambisonics. A focus is made on the practical implementation of such systems to account for the difficulties associated with causality and computational load. The latter are solved to propose an operational real-time adaptive system. Experimental results are reported and show effective noise attenuation for both methods.

Keywords: *Active Noise Control, Ambisonics, FPGA.*

**Corresponding author*: *loic.alexandre@ec-lyon.fr.*

1. INTRODUCTION

In the scope of sound field Active Noise Control (ANC), the control over an extended area is a key feature especially for practical applications. The use of multiple sources to generate the antinoise field and multiple microphones to control the resulting field is necessary. The classical approach using Multi-Point (MP) Filtered-x Least Mean Square (FxLMS) algorithm [1, 2] is effective but usually requires a large and uniform distribution of sensors. More recently with sound field synthesis, wave-domain approaches were introduced for spatial ANC [3–5]. Feedforward FxLMS algorithms based on spherical harmonic decomposition are an interesting alternative in particular through the possibilities of Spherical Microphone Arrays (SMAs) and loudspeaker arrays design. Although real-time implementations of such methods are rare due to their complexity, a few experimental results are reported in the literature [6, 7].

In this context, a primary study on Spherical Harmonics-based (SH) ANC processed on FPGA using the Faust programming language [1] is proposed. The SH-FxLMS algorithm is programmed with Faust and compile for the FPGA using the Syfala tool-chain [8]. A 4 inputs and 4 outputs ANC system is employed. The objective is to validate the SH-FxLMS algorithm and measure experimentally the noise reduction achieved around a 1st order ambisonics SMA. For comparison with the SH version of the algorithm, a MP-FxLMS algorithm is also implemented using the same ANC system.

[1] https://fast.grame.fr/

The outline of the paper is organized as follows: Section 2 provides the theoretical definition of both algorithms. In Sec. 3 the method for real-time implementation of the ANC algorithms is explained. Section 4 presents the experimental setup and the results obtained. Finally, Sec. 5 draws conclusions and suggests some perspectives.

2. THEORY

In this section, both feed-forward adaptive methods are explained in order to highlight their differences.

2.1 Pressure based FxLMS algorithm

Given the 4 inputs and 4 outputs configuration used in this study, the pressures measured at the $Q = 4$ microphones at a sample time n correspond to the error signals feeding the pressure-based FxLMS algorithm. The signals are described as a vector $\boldsymbol{e}_{\text{MP}} \in \mathbb{R}^{1\times Q}$ given by

$$\boldsymbol{e}_{\text{MP}}[n] = \boldsymbol{y}_p[n] + \boldsymbol{y}_s[n] \tag{1}$$

with $\boldsymbol{y}_p[n] \in \mathbb{R}^Q$ the sound field from the primary source and $\boldsymbol{y}_s[n] \in \mathbb{R}^Q$ the sound field from the secondary sources. For reference signal $x[n]$, the primary and secondary sound fields are defined as

$$\boldsymbol{y}_p = \mathbf{G}_p \boldsymbol{x}[n], \tag{2}$$

$$\boldsymbol{y}_s = \mathbf{G}_s \mathbf{H}_{\text{MP}}[n] \boldsymbol{x}[n] \tag{3}$$

with $\boldsymbol{x}[n]$ a buffer containing k samples of x. $\mathbf{G}_p \in \mathbb{R}^{Q\times k}$ and $\mathbf{G}_s \in \mathbb{R}^{Q\times S\times k}$ are respectively the primary and secondary acoustic paths from each source to each microphone. $\mathbf{H}_{\text{MP}}[n] \in \mathbb{R}^{S\times k}$ is the control filter at sample time n.

Minimizing the error signals power $\boldsymbol{e}_{\text{MP}}$ results in updating the filter $\mathbf{H}_{\text{MP}}$ as

$$\mathbf{H}_{\text{MP}}[n+1] = \mathbf{H}_{\text{MP}}[n] - \mu \boldsymbol{e}_{\text{MP}}[n] \widehat{\mathbf{G}}_s \boldsymbol{x}[n] \tag{4}$$

where μ is the convergence parameter and $\widehat{\mathbf{G}}_s$ the estimated secondary paths filters. The corresponding block diagram is presented in Fig. 1.

For this pressure-based FxLMS algorithm the control filter is a vector of S filters applied to each one of the secondary sources.

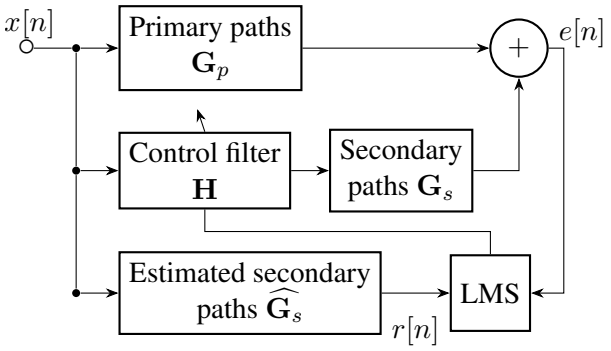

Figure 1. Block diagram of the multi-point FxLMS.

2.2 Spherical harmonics based FxLMS algorithm

In the case of the SH based FxLMS algorithm taken into account in this study, the error signals used for minimization are not the pressure signal of each microphone but the SH components obtained from the microphone signals [9, 10]. As a matter of fact, the baffled tetrahedral configuration of the 4 microphones allows to obtain the SH coefficients of the measured acoustic field up to the order $L = 1$ which corresponds to the first order ambisonics. The encoding matrix $\mathbf{E}$ used to obtain the SH coefficients is defined as

$$\mathbf{E} = \mathbf{F}^{-1} \mathbf{Q}_{lm}^T \tag{5}$$

where $(\cdot)^{-1}$ and $(\cdot)^T$ denote the inverse and the transpose respectively. The matrix of radial filters for baffled omnidirectional microphones at the order 1 is defined as $\mathbf{F} = \text{diag}(b_0(kr), b_1(kr), b_1(kr), b_1(kr))$ where

$$b_l(kr) = i^{-(l-1)}(kr)^2 h_l'^{(2)}(kr) \tag{6}$$

with the wave number $k = 2\pi f/c_0$, the SMA radius r and $h_l'^{(2)}(\cdot)$ the derivative of the spherical Hankel function of the second kind. The matrix $\mathbf{Q}_{lm} \in \mathbb{R}^{(L+1)^2\times Q}$ is obtained with the spherical harmonics $Y_{lm}(\phi_q, \theta_q)$ at each azimuthal ϕ_q and colatitude θ_q angle of the Q microphone.

The error signals $\boldsymbol{e}_{\text{SH}}[n] \in \mathbb{R}^{(L+1)^2}$ for the SH-FxLMS algorithm corresponding to the total sound field encoded using $\mathbf{E} \in \mathbb{R}^{(L+1)^2\times Q\times k}$ then becomes

$$\boldsymbol{e}_{\text{SH}}[n] = \mathbf{E}\left(\mathbf{G}_p \boldsymbol{x}[n] + \mathbf{G}_s \mathbf{H}[n] \boldsymbol{x}[n]\right). \tag{7}$$

The resulting update expression of the filter $\mathbf{H}_{\text{SH}}[n] \in \mathbb{R}^{k\times S\times(L+1)^2}$ is then

$$\mathbf{H}_{\text{SH}}[n+1] = \mathbf{H}_{\text{SH}}[n] - \mu \boldsymbol{e}_{\text{SH}}[n]\mathbf{E}\widehat{\mathbf{G}}_s\boldsymbol{x}[n]. \quad (8)$$

The block diagram of the algorithm is presented in Fig. 2.

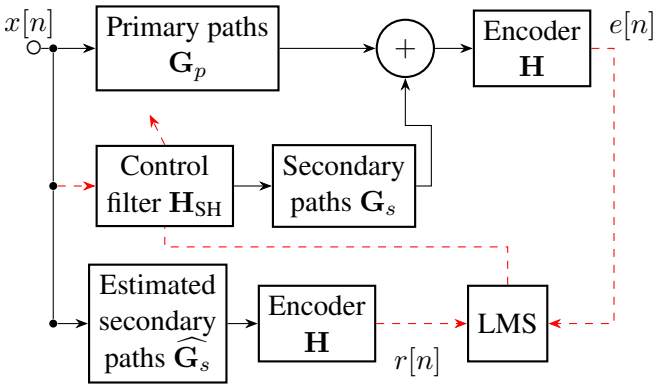

Figure 2. Block diagram of the spherical harmonics based FxLMS. The red dashed lines correspond to the spherical harmonics domain signals.

In this case, the adapted matrix of filters $\mathbf{H}_{\text{SH}}$ is the decoding matrix, also known as ambisonic decoder, enabling to obtain the secondary sources signals.

2.3 Normalization

For the two methods a normalization is applied to facilitate the setting of the convergence parameter. A fixed convergence parameter is set to $\mu_0 = 0.001$ and the step-size $\mu[n]$ is updated at each sample as in [11]. The step-size parameter is given by

$$\mu[n] = \frac{\mu_0}{||\boldsymbol{r}[n]||_2^2 + \boldsymbol{\beta}_e[n] + \delta} \quad (9)$$

with $||\boldsymbol{r}[n]||_2$ the ℓ_2-norm of the filtered-reference signal, $\delta = 1 \times 10^{-9}$ and $\boldsymbol{\beta}_e[n]$ the energy of the error signals $\boldsymbol{e}[n]$. The latter can be estimated in the iterative algorithm using a low-pass estimator as

$$\boldsymbol{\beta}_e[n] = \lambda\boldsymbol{\beta}_e[n-1] + (1-\lambda)\boldsymbol{e}^2[n] \quad (10)$$

where λ is set in the range $0.9 < \lambda < 1$. It is set to $\lambda = 0.9$ in the configuration studied here.

3. REAL-TIME IMPLEMENTATION

The real-time implementation of the algorithm is done using the Faust programming language on a FPGA. The programming of the FPGA is achieved using the Syfala toolchain [8] allowing the compilation of Faust audio DSP programs for AMD-Xilinx FPGAs. Since the objective is to implement the adaptive algorithms in real-time with Faust, all filters must be defined in the time domain. Another important point is the causality of each one of the filter. For the SH-FxLMS algorithm, an option is to define the control filter as a vector of filters [12] and use a Near-Field Compensated ambisonic decoder. However, time version of such decoders does not compensate the loudspeakers delay of propagation to stay causal, which is an issue for real-time active noise control. Another option, which is the one chosen in this study, is to set the control filter $\mathbf{H}_{\text{SH}}$ as the ambisonic decoder [13–15]. Therefore, the control filter $\mathbf{H}_{\text{SH}}$ and the estimated secondary paths $\widehat{\mathbf{G}}_s$ are defined with Finite Impulse Response (FIR) filters. The performance of the FPGA and the optimization process of the current Syfala v0.7.1 toolchain version do not yet permit to use FIR filters with a large number of taps. Consequently, $S \times Q$ 2-taps FIR filters are used for $\widehat{\mathbf{G}}_s$, S 4-taps FIR filters for $\mathbf{H}_{\text{MP}}$ and $S \times (L+1)^2$ 4-taps FIR filters for $\mathbf{H}_{\text{SH}}$. Due to this filter configuration, only monochromatic reference signals are used for this practical study. The 2-taps FIR filters are computed such that their z-transform evaluated for $z = e^{i2\pi f/fs}$ and $z = e^{-i2\pi f/fs}$ equals the Discrete Fourier Transform of the measured secondary acoustic paths $\mathbf{G}_s$ at frequency f. The encoding matrix of Eq. 5 is implemented using a constant matrix $\mathbf{Q}_{lm}$ and a biquadratic IIR filters for $\mathbf{F}$.

In Fig. 2, the input signal of the control filter $\mathbf{H}_{\text{SH}}$ has to be an ambisonic signal. In practice, this signal corresponds to an estimation of the reference noise signal which could, for example, be obtained from a reference SMA located close to the source. However, in this study the reference signal is known and generated from the ANC system which allows to use it as the reference for each one of the $(L+1)^2 = 4$ SH components.

4. EXPERIMENTS AND RESULTS

4.1 Experimental layout

The experimental study is carried out at the Laboratory of Fluid Mechanics and Acoustics inside a listening room of dimensions $[3, 4, 2.7]$ m, presented in Figs. 3 and 4. The listening room has an overall reverberation time of 0.14 s.

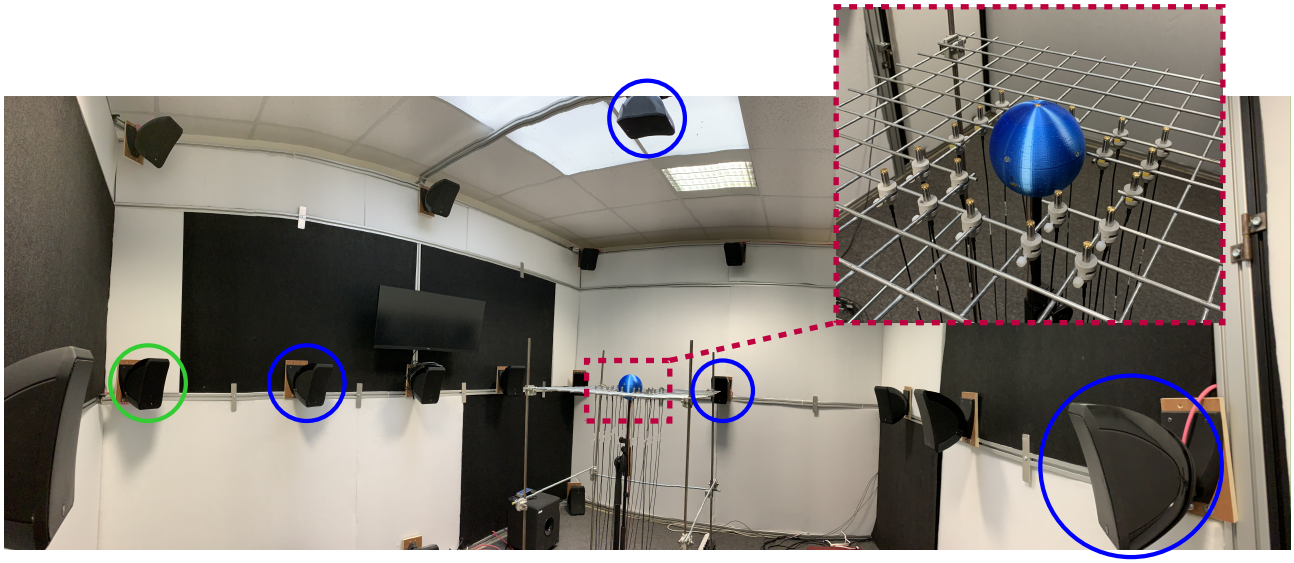

Figure 3. Picture of the experimental setup inside a listening room with the control spherical microphone array and the measurement microphone array at the center of the room. The loudspeakers used as secondary and primary sources are indicated with blue and green circles respectively.

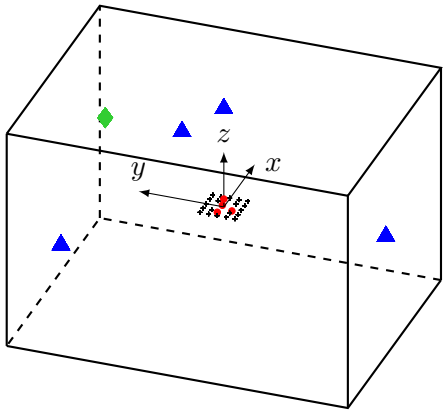

Figure 4. Scheme of the experimental installation with (♦) a primary source, (▲) 4 secondary sources, (●) 4 control microphones in a tetrahedral configuration inside a sphere of radius 5 cm and (+) 20 measurement microphones.

The experimental configuration used for the active noise control is composed of 5 *Focal* ® Sib loudspeakers, 1 for the primary source and 4 for the secondary sources, as shown in Fig. 4. The control microphone is a spherical microphone array with 4 *B&K* ® Type 4958 microphones connected to 4 *B&K* ® Type 1708 IEPE power supply. The 5 cm radius rigid sphere is 3D printed. The speakers and the microphones are connected to the Genesys ZU-3EG *Zynq* ® Ultrascale+ through 3 *Analog devices* ® ADAU1777 audio codecs. The FPGA and the audio codecs are the processing system which acquires 4 microphone input signals and produces 6 signals: the 4 secondary signals, the reference signal for the primary source and the error signal. To program and control the FPGA board with Faust, the syfala toolchain is used on a dedicated computer. The sampling frequency is set to 8000 Hz for the ANC system.

Surrounding noise measurement is carried out with a 20× *B&K* ® Type 4958 microphones array arranged in a horizontal plane around the control SMA as presented in Fig. 3. The microphone mounting grid is zero-centered and has a 5 cm spacing which is significantly smaller than the wavelengths of the signals considered. Due to their support, the microphones are offset by 5 mm from the grid. The signal acquisition of the planar array is done using a *National Instruments* ® cDAQ-9178 and 5 NI 9234 modules at a sample rate of 6400 Hz. The acquisition is performed with Python on a different computer than the one used for the FPGA programming. The measurement

microphone array as well as the equator of the spherical microphone array are located at the center of the room and at a height of 1.2 m.

4.2 Protocol

The secondary paths are identified using an exponential sine sweep method [16]. The Impulse Response measurements are performed using a *Ferrofish* ® A32 sound card at a sampling rate of 32000 Hz and the acquisition is done with a Python script. The signals from the microphones go through the FPGA and the audio codecs programmed with a bypass, which allows to include the response of the ANC system into the IRs. The transfer function of the *Ferrofish* ® sound card is simultaneously measured and compensated in the IR measurements.

The reference signal x is a monotone sine signal generated by the FPGA at different frequencies. As in [6] the reference signal is then known since the estimation of the noise source is not of interest in this study.

A 10 s acquisition using the 20 microphones array is made only with the primary source playing. Then the ANC is started and the error signal from the algorithm is visualized in real time on an oscilloscope. Another 10 s acquisition is performed only after the convergence is monitored with the error signal attenuation.

4.3 Multi-point FxLMS

The noise reduction performance for the multi-point FxLMS algorithm are is measured using the 20-microphone array around the spherical control microphone array.

In order to compare the noise reduction on the SMA surrounding area for different frequencies, the Regional Noise Reduction (RNR) is introduced based on [12] such that

$$\varepsilon = 20\log_{10}\left(\frac{\sum_{i=1}^{Q}|p_p(\boldsymbol{x}_i)|}{\sum_{i=1}^{Q}|p_t(\boldsymbol{x}_i)|}\right) \tag{11}$$

with p_p the spectrum of the primary sound field and p_t the spectrum of the total sound field after convergence of the FxLMS algorithm.

Results of RNR using the multi-point method for different frequencies are presented with dots data points in Fig. 5. Two different cases are reported for the multi-point method, the RNR using all the 20 measurement microphones and only the four microphones closest to the SMA represented with solid line and dashed line respectively.

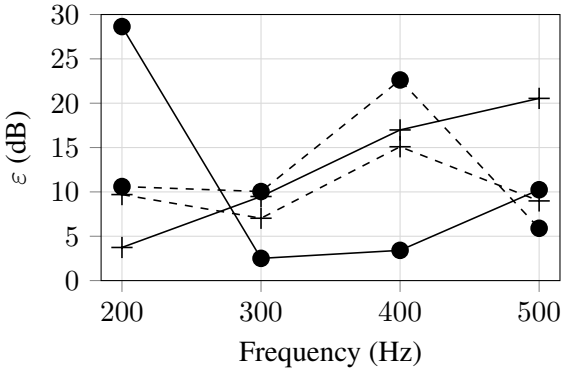

Figure 5. Regional noise reduction using (●) multi-point and (+) spherical harmonics methods for different frequencies. The calculation is performed with (___) the 20 measurement microphone signals for global noise reduction and (_ _ _) only with the 4 measurement microphones closest to the center for proximity noise reduction.

On one hand, the resulting RNR using the 20 measurement microphone signals appears to be low, around 4 dB, for the cases at 300 Hz and 400 Hz. However, it is larger when taking into account only the signals from the 4 microphones closest to the center. On the other hand, a RNR of 10 dB and 28 dB is achieved for frequencies 500 Hz and 200 Hz respectively.

The second row in Fig. 6 presents the resulting sound field after convergence of the MP-FxLMS. For comparison, the primary sound field before ANC is presented on the first row. The results at 200 Hz, 300 Hz, 400 Hz and 500 Hz are presented from left to right and the data between the measurement points is obtained using linear interpolation.

One can observe that the noise reduction is not completely homogeneous on the whole area surrounding the SMA. For the reference signal at 200 Hz in particular, a zone with important attenuation is achieved on one side of the control SMA. The latter appears to be the area with the highest energy on the corresponding primary sound field. Although the reduction is less important for the other frequencies, the same behavior seems to occur in the case of the multi-point method.

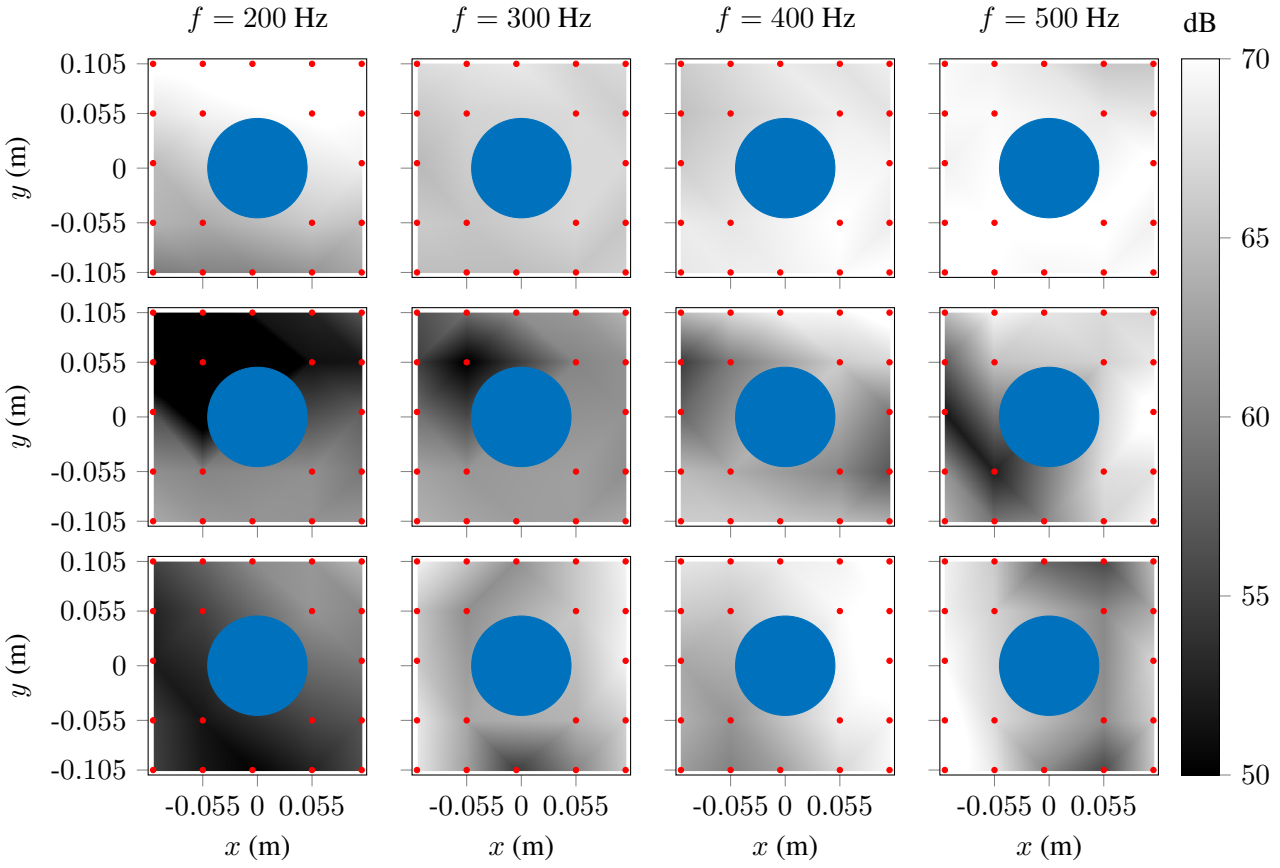

Figure 6. (First row) Primary sound field and total sound field using (second row) the multi-point and (third row) the spherical harmonics methods for sine signal at different frequencies. Linear interpolation is used for data between the microphone data points marked with red dots. The spherical microphone array is indicated with a blue disc at the center.

4.4 Spherical harmonics FxLMS

In the case of the spherical harmonics based FxLMS algorithm, Fig. 5 shows a RNR between 7 dB and 15 dB when taking into account the four microphones closest to the SMA. However, the RNR obtained with the 20 microphones is low, around 3 dB, at the frequency $f = 200$ Hz. While the RNRs obtained with only the four closest microphones seem to same behavior for both methods, the total RNR at each frequency varies significantly.

The total sound fields obtained from the primary and secondary sources are presented on the third row in Fig. 6. Results show a reduction on different areas compared to the multi-point method, especially at 200 Hz and 500 Hz. Since the SH-FxLMS update is based on the SH components of the sound field, the noise reduction does not seem to be focused on the high energy areas in this case. Therefore, at 200 Hz for example, the noise reduction using the SH method is not as significant but is more uniform than for the multi-point one.

Although the noise attenuation obtained with the SH-FxLMS algorithm validates the method, the disparity of the RNRs obtained makes both methods difficult to compare. If the spherical harmonics method seems to give better results on the whole area of measurement, it is the opposite at the frequency $f = 200$ Hz. Moreover, a theoretical encoding matrix for a rigid SMA is used for the SH-FxLMS and the calibration of the control SMA might improve the performance of the ANC system.

5. CONCLUSION

In this paper, initial results of a practical spherical harmonic-based and multi-point ANC system are proposed. Two FxLMS algorithms are programmed with the Faust programming language and compiled for a FPGA using the Syfala tool-chain. As a primary experiment, a basic 4 microphones along with 4 loudspeakers configuration is deployed. The control microphone consists of a baffled tetrahedral SMA which allows the expansion of the measured acoustic field up to the first order ambisonics. The possible issues of a real-time implementation of such a time-domain feedforward FxLMS algorithms are addressed especially for the SH version. In order to measure the sound field around the control microphone after convergence of the algorithm, an array of 20 microphones is set. Results of RNR show that both methods achieve noise reduction at the four measured frequencies. In the vicinity of the SMA the attenuation is similar and significant. However, the SH-FxLMS algorithm gives better results for the highest tested frequencies. A theoretical investigation would be of interest to study the limits of robustness for both algorithms and compare the resulting noise reduction. Future works include noise reduction over a wider frequency range and the implementation of a more complex ANC system with a larger number of sensors depending on the future optimization progress of the FAST programming workflow.

6. ACKNOWLEDGMENTS

This work was supported by the French National Research Agency, ANR FAST (ANR-20-CE38-0001).

This work was carried out within the LABEX CeLyA (ANR-10-LABX-0060) of the University of Lyon.

7. REFERENCES

[1] S. Elliott, I. Stothers, and P. Nelson, "A multiple error lms algorithm and its application to the active control of sound and vibration," *IEEE Transactions on Acoustics, Speech, and Signal Processing*, vol. 35, no. 10, pp. 1423–1434, 1987.

[2] J. Zhang, T. D. Abhayapala, P. N. Samarasinghe, W. Zhang, and S. Jiang, "Multichannel active noise control for spatially sparse noise fields," *The Journal of the Acoustical Society of America*, vol. 140, no. 6, pp. EL510–EL516, 2016.

[3] N. Epain and E. Friot, "Active control of sound inside a sphere via control of the acoustic pressure at the boundary surface," *Journal of sound and vibration*, vol. 299, no. 3, pp. 587–604, 2007.

[4] P. Peretti, S. Cecchi, L. Palestini, and F. Piazza, "A novel approach to active noise control based on wave domain adaptive filtering," in *2007 IEEE Workshop on Applications of Signal Processing to Audio and Acoustics*, pp. 307–310, IEEE, 2007.

[5] Y. Maeno, Y. Mitsufuji, P. N. Samarasinghe, N. Murata, and T. D. Abhayapala, "Spherical-harmonic-domain feedforward active noise control using sparse decomposition of reference signals from distributed sensor arrays," *IEEE/ACM Transactions on Audio, Speech, and Language Processing*, vol. 28, pp. 656–670, 2019.

[6] H. Sun, T. D. Abhayapala, and P. N. Samarasinghe, "A Realistic Multiple Circular Array System for Active Noise Control Over 3D Space," *IEEE/ACM Transactions on Audio, Speech, and Language Processing*, vol. 28, pp. 3041–3052, 2020.

[7] S. Ha, J. Kim, H.-g. Kim, and S. Wang, "Horizontal active noise control-based wave field reproduction using a single circular array in 3d space," *Applied Sciences*, vol. 12, no. 20, p. 10245, 2022.

[8] M. Popoff, R. Michon, T. Risset, Y. Orlarey, and S. Letz, "Towards an FPGA-Based Compilation Flow for Ultra-Low Latency Audio Signal Processing," in *SMC*, (Saint Étienne), 2022.

[9] B. Rafaely, *Fundamentals of Spherical Array Processing*, vol. 16 of *Springer Topics in Signal Processing*. Cham: Springer International Publishing, 2019.

[10] J. Ahrens, *Ambisonic Encoding of Signals From Spherical Microphone Arrays*. 2022.

[11] M. Akhtar and W. Mitsuhashi, "A modified normalized FxLMS algorithm for active control of impulsive noise," *European Signal Processing Conference*, 2010.

[12] Y. Maeno, Y. Mitsufuji, P. N. Samarasinghe, N. Murata, and T. D. Abhayapala, "Spherical-Harmonic-Domain Feedforward Active Noise Control Using Sparse Decomposition of Reference Signals from Distributed Sensor Arrays," *IEEE/ACM Transactions on Audio, Speech, and Language Processing*, vol. 28, pp. 656–670, 2020.

[13] H. Sun, T. D. Abhayapala, and P. N. Samarasinghe, "Time Domain Spherical Harmonic Analysis for Adaptive Noise Cancellation over a Spatial Region," in *ICASSP 2019 - 2019 IEEE International Conference on Acoustics, Speech and Signal Processing (ICASSP)*, pp. 516–520, 2019.

[14] J. Zhang, W. Zhang, J. Zhang, T. Abhayapala, and L. Zhang, "Spatial Active Noise Control in Rooms Using Higher Order Sources," *IEEE/ACM Transactions on Audio, Speech, and Language Processing*, vol. PP, pp. 1–1, 2021.

[15] S. Koyama, J. Brunnström, H. Ito, N. Ueno, and H. Saruwatari, "Spatial Active Noise Control Based on Kernel Interpolation of Sound Field," *IEEE/ACM Transactions on Audio, Speech, and Language Processing*, vol. 29, pp. 3052–3063, 2021.

[16] A. Farina, "Simultaneous Measurement of Impulse Response and Distortion with a Swept-Sine Technique," Audio Engineering Society, 2000.